Proceedings of Fifth International Conference on **Enhanced, Compact and Ultra-Compact Heat Exchangers: Science, Engineering and Technology**, Eds. R.K. Shah, M. Ishizuka, T.M. Rudy, and V.V. Wadekar, Engineering Conferences International, Hoboken, NJ, USA, September 2005.

CHE2005 – 22

MICRO AND MESO SCALE COMPACT HEAT EXCHANGERS IN ELECTRONICS THERMAL MANAGEMENT-A REVIEW

Yogendra Joshi and Xiaojin Wei

G.W. Woodruff School of Mechanical Engineering
Georgia Institute of Technology
Atlanta, GA 30332
Yogendra.joshi@me.gatech.edu

ABSTRACT

Due to dramatic gains in functionality and speed, microelectronic components are experiencing ever increasing heat fluxes. Microprocessor heat fluxes are approaching 100W/cm^2 on a spatially averaged basis on the chip of typical footprint area 1-5 cm^2, with several times larger values locally in the logic regions. Power electronics devices are approaching heat fluxes in the 1 kW/cm^2 range over footprint areas of 10 cm^2 or higher. Proper operation of the semiconductor devices typically requires maximum temperatures to be limited below 85-100^{o}C for microprocessors and 125^{o}C-150^{o}C for silicon based power electronics components.

During the past two decades dramatic advances have been made in microfabrication techniques. Many of the same manufacturing techniques developed for the fabrication of electronic circuits are being used for the fabrication of compact heat exchangers. In this paper we will review the advances in the fabrication and characterization of micro and meso scale compact heat exchangers for electronics thermal management, with a focus on the past decade. The review will focus primarily on single phase liquid cooling and two-phase cooling. A systems perspective will be taken, which involves transferring the heat generated in the electronic components through a path involving multiple media, leading to its ultimate rejection. Since this rejection is to ambient air for most ground based electronic equipment, liquid cooling schemes require a remote liquid-to-air heat exchanger, whose size and efficiency ultimately determine the size of the overall cooling system.

Capabilities and characteristics of microfabrication and bonding techniques play a key role in the development of such devices. A discussion of the state-of-the-art microfabrication techniques will be included, and the current research challenges identified. Fluidic pumping is often required for both single phase and two phase devices. The current status of these technologies is discussed.

A number of new effects in the physics of transport phenomena have been identified by various researchers in meso-sized thermal management devices. These are discussed over the range of feature sizes studied. Remaining gaps in the understanding of these phenomena are identified.

1 INTRODUCTION

While the clock speed and capabilities of microprocessors have increased dramatically over the past decade in accordance with the Moores's Law, the *system sizes* for a given product segment utilizing these devices, such as laptops, desktops, and high performance servers have either stayed the same or shrunk. This has resulted in a multi-fold increase in the heat dissipation requirements at the system level. These increases have been handled using air-cooled heat sinks of increasing size and/or larger air flow rate fans. The most common architecture has been of an integrated heat sink (IHS) directly attached to the back side of a processor chip or heat spreader, using a thermal interface material (Fig. 1).

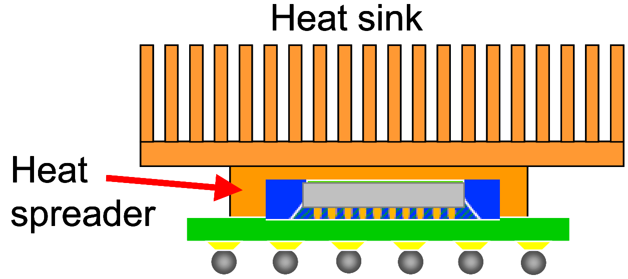

Fig. 1 *A flip chip package with an integrated air cooled heat sink*

Continued growth in heat sink sizes and air speeds to handle higher chip powers are limited by the available system real estate and the acoustic noise requirements respectively. Fig. 2 shows the heat sink volumes for several generations of microprocessors.

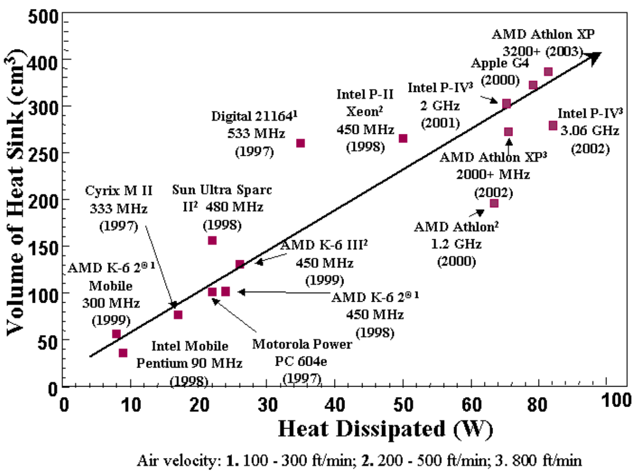

Fig. 2 *Increasing sizes of air cooled heat sinks for successive generations of microprocessor chips.*

The choice of thermal management solutions is further constrained by the highly non-uniform distribution of heat flux on the chip surface (for example, Viswanath et al. (2000)). This arises due to the location of the low power regions associated with the memory on the same chip (or die) as the high power regions associated with the logic blocks. Such "hot spots" are not effectively handled by air cooling techniques. In the absence of any hot spots, Fig. 3 shows the state-of-the-art power dissipation capability of a 1 cm x 1 cm chip to be ~70 W, using an air cooled IHS, with an assumed overall thermal resistance of 0.33 K/W, ambient temperature of 45°C, and a maximum allowable chip temperature of 85°C. As the hot spot loading factor, the ratio of the peak to the mean heat flux increases, the heat removal ability of the IHS is sharply reduced. The overall heat removal rates and the ability to handle non-uniform heating are significantly better for a stacked microchannel based liquid cooling scheme, to be discussed later in this paper.

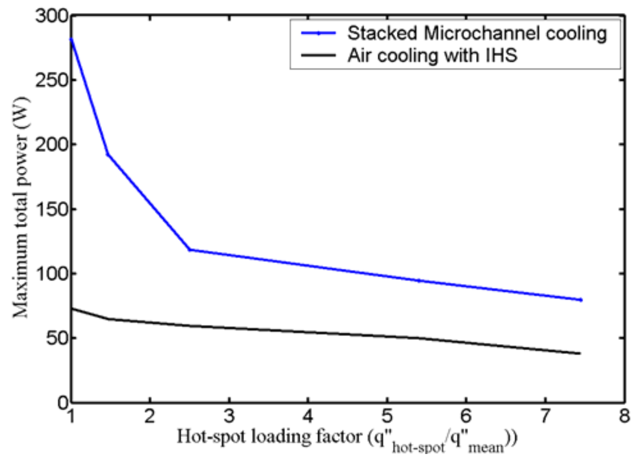

Fig. 3 *The maximum heat dissipation capability of a chip with an air cooled integrated heat sink, and a stacked microchannel liquid cooling device, as a function of the chip heat flux non-uniformity.*

A number of other emerging features in microprocessor design are likely to significantly impact thermal management. The need for high speed chip-to-chip signal transmission is driving the research on optical interconnects. Associated requirements for optical access may further limit the surface area available for attachment of thermal management devices. Also, heat generation in the wiring or interconnects between the semiconductor devices within a chip is fast becoming a concern. As the feature sizes reduce to ~20 nm within the next decade, the electrical resistance of the interconnects will increase dramatically. With no reduction in the current densities, this will result in a significant increase in Joule heating within the chip wiring, further exacerbating the thermal management problem. Also, the needs to reduce signal transmission delays and provide multi-function integration benefits are driving an interest in three-dimensional circuit architectures. Such stacking of active layers significantly increases the heat removal requirements, with limited available surface area.

While the above discussion focuses on microprocessor architectures, many of the thermal management concerns are also shared by other types of devices such as power electronics, radio frequency amplifiers, and opto-electronics. Heat fluxes of 1 kW/cm^2 or higher have been projected in power electronics applications. In opto-electronics a very precise control of the laser temperature is necessary in order for the device to operate properly.

The present paper reviews the advances made in high heat flux chip cooling, with a focus on the past decade. These devices have heat flux requirements between 75 W/cm^2 and 1 kW/cm^2, and need to maintain maximum chip temperatures in the range of 85-100°C for microprocessors, and 125°C-150°C for silicon based power electronics components. Heat is transferred in these devices near the chip by single phase liquid cooling, or by liquid to vapor phase change. The ultimate rejection to the ambient involves a single phase liquid to air heat exchanger, or condenser. One of the major facilitators of recent advances has been the wide availability of a variety of microfabrication methods utilized in semiconductor fabrication. This has enabled the development of *micro and mesoscale* cooling systems with overall sizes between 10^0 and 10^1 cm^3, incorporating cooling passage features between 10 and 100 µms. For geometrical characterization, in this review, we define micro-scale features to span 10–100 µm, and meso-scale from 100 µm-1 mm.

2 MESOSCALE LIQUID COOLING OF ELECTRONICS

As seen in the previous section, a continuing increase in air cooled heat sink sizes is required to handle the high chip heat fluxes. This is infeasible due to the tightly limited space available for a thermal management device around a typical electronic chip within an enclosure, particularly for portable systems. An alternative is to utilize a compact heat exchange device to transfer the heat from the chip to a working fluid. The working fluid in liquid or vapor form is then carried to a remote heat exchanger, placed within the system at a location where space availability is at a lesser premium. Upon heat rejection to the ambient, the working fluid is returned to the chip-to-fluid heat exchanger. This overall scheme, also referred to as a flow loop, is illustrated in Fig. 4. A key expectation in such an implementation is that in addition to solving the real estate constraint, the overall thermal resistance achievable is lower than with a directly attached air-cooled heat sink.

A number of studies within the past decade have investigated mesoscale flow loops for chip cooling. There are three major components of such thermal management systems: the chip to fluid heat exchanger, the remote heat exchanger, and the fluid pumping mechanism. Considerable effort has been focused during the past decade by various investigators in miniaturizing these components using microfabrication techniques. A review of some of these efforts is the main theme of this paper. Both fabrication techniques and the thermal characterization of these system components are addressed. We conclude with a perspective on future research directions for mesoscale thermal management systems for electronics cooling.

2.1 Chip to Fluid Heat Exchanger

2.1.1 Working Fluids:

Two types of working fluids have been used in the flow loops employed in electronics cooling. Water has been used in single phase cooling due to its superior specific heat and thermal conductivity. For a maximum chip temperature limit of 85°C, the use of water in a phase change cooling scheme requires sub-atmospheric operation in order to reduce the saturation temperature below 100°C. Perfluorinated fluids have been employed for phase change cooling of electronics due to a range of available boiling points. These liquids are also electrically inert, which is desirable in the event of accidental leakage. As listed in Table 1, compared with water, these fluids have thermal conductivity of one order of magnitude lower, specific heat of one fourth , and surface tension almost an order of magnitude lower.

Property	FC-87	FC-72	FC-84	Water
Boiling point, °C	30	56	83	100
Specific Heat, J/kg-K	1088	1088	1130	4184
Thermal conductivity, W/m-K	0.055	0.0545	0.0535	0.68
Surface tension, N/m	8.9×10^{-3}	8.5×10^{-3}	7.7×10^{-3}	5.9×10^{-2}
Dynamic viscosity, kg/m-s	4.2×10^{-4}	4.5×10^{-4}	4.2×10^{-4}	2.7×10^{-4}

Table 1 *Thermophysical Properties of Perfluorinated Liquids Compared to Water*

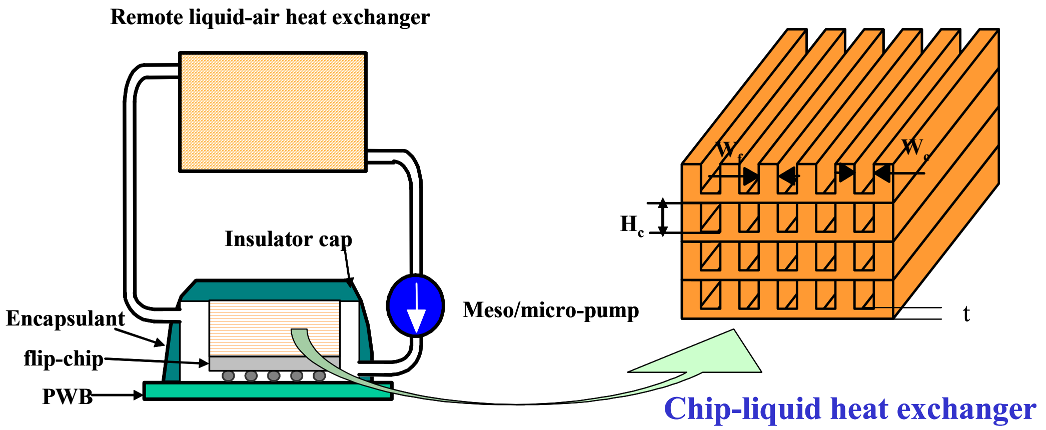

Fig. 4 Meso-scale flow loop configuration for electronics thermal management applications. A buoyancy driven implementation does not utilize the pump

2.1.2 Fabrication:

Both traditional fabrication and micromachining techniques have been applied to fabricate meso-micro scale heat exchangers. Precision mechanical machining using CNC mill was used by Qu and Mudawar (2002) to fabricate microchannels in a copper substrate. The typical feature size available by CNC milling is around several hundred micrometers. Ramaswamy et al. (1999a) used a wafer dicing saw to cut channels in silicon wafers. Under optimized cutting conditions channels as narrow as 30 μm can be achieved with minimal chipping. For hard materials, laser beams can also be used to drill holes and make rectangular cuts in the substrate. Typically hole diameters of several hundred micrometers can be expected from laser micromachining. The main challenges with laser micromachining are the recasting of residuals, heat affected zone and micro-cracks caused by excessive temperature gradient. Zhu et al. (2002) described a mixed ablation mode to minimize the heat affected zone. For certain conducting substrates, electro-discharge machining can be used to cut channels (Saito, 1984). These traditional fabrication methods offer the simplicity of operation with acceptable accuracy for meso-scale heat exchangers. For micro-scale heat exchangers, the more stringent geometric constraints make it necessary to utilize micromachining techniques.

In general, micromachining techniques can be categorized as bulk machining, surface machining and others. Bulk micromachining is probably the most used technique for micro scale heat exchangers. It involves patterning the substrate such as silicon wafers with chemical etching or physical ion bombardment or both. Wet etching has been widely used to etch grooves in silicon. Ramaswamy et al. (1999b) etched microchannels in <110> silicon wafers using 44% KOH solution at 85^{o}C. Wet etching is typically orientation dependent; thus, it is not suitable for creating complex geometries.

One of the promising dry etching techniques is Deep Reactive Ion Etching (DRIE). In a typical Bosch process, three steps are cycled to achieve the required trench depth. The three-step process starts with etching of silicon followed by polymer deposition which protects the sidewall of the trench. In the third step, the polymer on the trench bottom is removed. Aspect ratios as high as 10 have been achieved using the process Chen et al. (2002). Wei et al. (2005) fabricated multi-layers of microchannels and flow vanes in silicon wafers using DRIE technique. These layers were then bonded into a stacked using silicon to silicon direct bonding. The typical fabrication steps are listed in Figure 5.

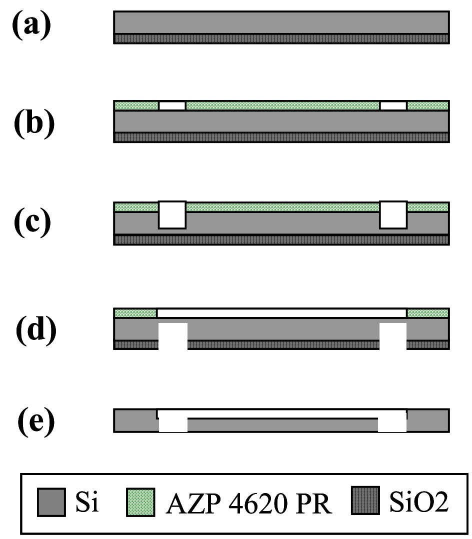

Fig. 5 Illustration of the typical fabrication steps for stacked microchannel heat exchanger (Wei et al., 2005)

As shown in Fig 5 (a), the process started with the deposition of a thick layer of SiO_2 on the backside of a double-polished silicon wafer. The purpose of the SiO_2 layer was to protect the backside of the wafer from scratches and contaminations. In step (b), 14 μm positive photo-resist AZP 4620 was spun on the front side of the wafer and patterned using a standard photo-lithography process in a Karl-Suss MA6 mask aligner (h-line). The exposed wafer was developed in 1:3 diluted AZ400K developer. Before the Bosch process the photo-resist was fully baked as required by the ICP machine. This caused photoresist reflow and loss of pattern fidelity. After the front-side etching was done in step (c), the photoresist was removed in heated SHIPLEY MICROPOSIT remover 1165A. Silicon dioxide was then removed from the backside after step (c). The wafers were then flipped such that subsequent processes were conducted on the front-side of the wafers. After thorough clean in Piranha solution, silicon dioxide was deposited by PECVD on the front-side of the wafer to protect the surface for future bonding. An AZP 4620 photolithography was performed for the backside of the wafer. Openings were made for both headers and microchannels which allowed ICP etching from the backside as shown in step (d). After the headers were etched through, silicon dioxide and photoresist were stripped-off and the wafers were cleaned in Piranha again.

It is noted here that during ICP etching the wafer was cooled from the backside by Helium flow. This is important in order to protect the photo-resist integrity. When there are through features, there will be helium leakage which can cause the machine to shut-down as helium pressure is not able to be maintained. To prevent this, the working wafer was bonded to a carrier wafer using either thin photoresist or thermal conducting grease. Following similar steps, the manifolds and fluid connection holes are also fabricated on silicon wafers. In the end, five component layers were fabricated in silicon, as shown in Figure 6 (Wei et al., 2005). These individual layers were then bonded into a stack using silicon-silicon direct bonding.

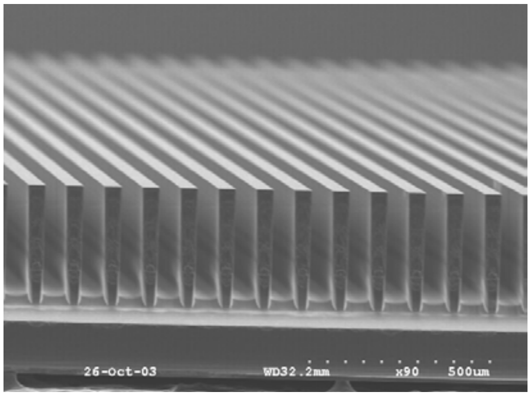

(a) Microchannel array

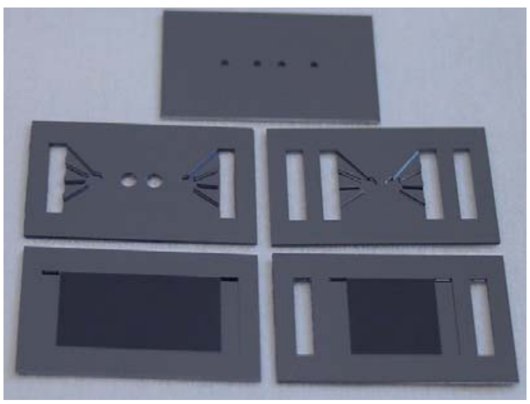

(b) All five layers fabricated in Silicon

Fig. 6 Samples fabricated using DRIE (Wei et al., 2005)

A typical bonding procedure started with wafer cleaning. The standard CMOS cleaning processes, RCA-I and RCA-II cleaning, were initially considered to remove organic particles and metals from the wafer surface respectively. However, it was found that RCA cleaning was not sufficient to remove polymer residuals formed during the DRIE etching. Piranha solution consisting of 3 H_2SO_4 and 1 H_2O_2 by volume was found to be very effective in removing the organic contamination. SEM pictures taken before and after Piranha cleaning show that the polymer residuals left in the Bosch process were significantly less. After a thorough DI water rinse, the wafer was dipped in dilute 1% high-purity HF for 15 seconds and then rinsed in DI water. The wafer was then treated in a RCA-I solution for about 10 minutes to achieve a hydrophilic surface and the diced chips are subsequently brought together to initiate room temperature bonding. A Teflon jig was built to help align the silicon chips by flushing all the edges of the chips against three posts in the Teflon jig. After the chips were aligned properly, a small pressure was applied at the center of the chips to initiate the bonding. The bonded structure was then examined using an infra-red imaging system. Following the room temperature bond, a two-step annealing process was implemented to enhance the bonding strength. The bonded structure was first heated at around 500^{o}C in air with a large pressure (~32 Psi) applied by metal block followed by a one hour post-annealing inside a N_2 furnace. The bonded structure passed hydraulic test and further thermal tests confirmed that the interface resistances between layers were negligible.

An attractive alternative to bulk micromachining is surface micromachining where structural layers are added onto the substrate. Sophisticated structures can be achieved using sacrificial layers. For micro-heat-exchangers, regular surface micromachining cannot produce channels deeper than a few μms due to the limit in the film thickness; however, advances in thick photoresist or photo-definable and decomposable polymers now make it possible to form thick sacrificial layers. Papausky et al. (1998) developed a low-temperature IC compatible process to fabricate metallic microchannels on silicon and glass substrate. Nickel was used as the structure materials while the inner surface of the channels were coated with gold. The fabrication process included an initial deposition of metal layers to form the bottom wall of the rectangular channel. A sacrificial layer of AZP 4620 thick photoresist was spun-on and patterned. Sidewalls and top walls were formed in an electroplating process. Upon soaking in acetone bath, the sacrificial photoresist layer was removed to form the microchannels. Microcannels have been fabricated with 30 μm to 1.5 mm in width, 0.5 mm to several centimeters in length, and 5–100 μm in thickness. The wall thickness ranged from 5 to 50 μm.

An emerging etching technique is electrochemical etching which has been used to fabricate porous silicon and tailored for microchannel fabrication in Lehmann (1993). Extremely high aspect ratio channels can be produced (Foll et. al., 2002).

3 PERFORMANCE CHARACTERIZATION

3.1 Single Phase Implementations

Following the work of Tuckerman and Pease (1981) many studies have been conducted to characterize the thermal and hydraulic performance of the microchannel devices. A comprehensive review of this subject can be found in Mehendale et. al., (1999). Some recent work will be described here.

As indicated in Mehendale et. al. (1999), several studies found that the Nusselt numbers and friction factors for microchannels deviate from predicted values based on theories or correlations for macro-scale channels. Unfortunately, there is little consensus in the literature. Xu et al. (2000) reported that flow characteristics in microchannels with hydraulic diameter of 30 to 344 μm at Reynolds numbers of 20 to 4000 agree with predictions based on the Navier-Stokes equation. Liu and Garimella (2002) showed that conventional correlations offer reliable predictions for laminar flow characteristics in microchannels over a hydraulic diameter range of 244 to 974 μm. Recently, Lee and Garimella (2003) investigated heat transfer in microchannels made of copper for a Reynolds number range of 300 to 3500. The widths of the studied channels range from 194 μm to 534 μm, while the depths are five times the widths. In deducing the average Nusselt number, an average wall temperature based on a one-dimensional conduction model was used. For laminar flow the measured Nusselt number agreed with predictions for thermally developing flow over the entire length of the channel.

Baviere et al. (2004) studied flow inside smooth and rough microchannels with height range of 7 μm to 300 μm and Reynolds number range of 0.01 to 8000. In the smooth wall case, the friction factor was well predicted by theory. For the rough wall case, an artificial surface roughness was added to the sidewalls of the smooth microchannels and the measured friction loss was significantly larger but no earlier transition to turbulence was observed. Sharp et al. (2000) employed Micro-PIV techniques to study transition to turbulence in microtubes with a range of diameters from 184 μm to 242 μm. The measured centerline velocity was compared with predictions to identify the possible transition to turbulence. Zeighami et al (2000) studied transition to turbulence in rectangular microchannels with a depth of 150 μm and width of 100 μm. Instantaneous vectors of velocity were obtained for different Reynolds numbers by Micro-PIV measurement. At a Reynolds number of 1600, temporally fluctuating asymmetric velocity was observed, and this was identified as the transition.

A stacked microchannel heat exchanger was developed for electronics cooling (Wei et al., 2004). A prototype heat exchanger was fabricated using the processes described earlier. A schematic of the prototype is shown in Fig. 7. The five-layer structure includes two bottom microchannel layers, two manifold layers and one top layer providing the fluid connection ports to external loop. On the backside of the chip, thin film heaters and sensors are deposited to provide heating and temperature sensing respectively. The flexible design of the prototype allows both counter-flow and parallel flow arrangement. The thermal performance for both arrangements were measured in a close-loop setup. As indicated in Fig. 8, at low flow rate the total thermal resistance, defined as the ratio of the maximum temperature difference to the input power, for a counter-flow arrangement produces slightly larger thermal resistance than parallel flow arrangement; whereas, at higher flow rate, the difference between the two configurations is negligible. This is due to the negative heat flux occurring near the ends of the channel for counter-flow cases where heat is being rejected from the hot water to the surrounding cooler silicon wall. At high flow rate, this effect is significantly less. Overall thermal resistance of less than 0.1 ^{o}C/W has been achieved for both counter-flow and parallel flow, suggesting significant improvement over current air-cooling technology while maintain a very low profile (1”x1”x0.1”).

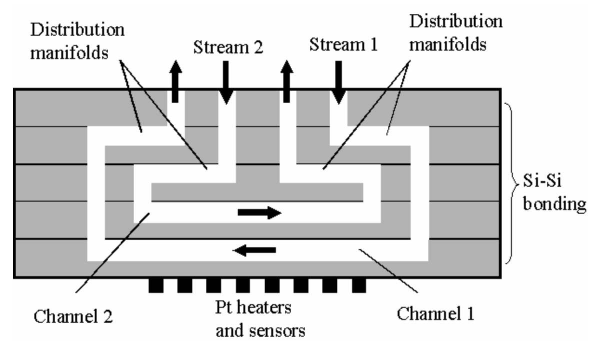

(a) A counter-flow configuration

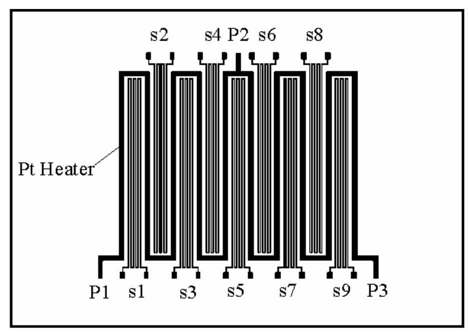

(b) Backside heater and sensor patterns

Fig. 7 Schematic of a stacked microchannel heat exchanger with integrated on-chip manifolds and temperature sensors (Wei et al., 2004)

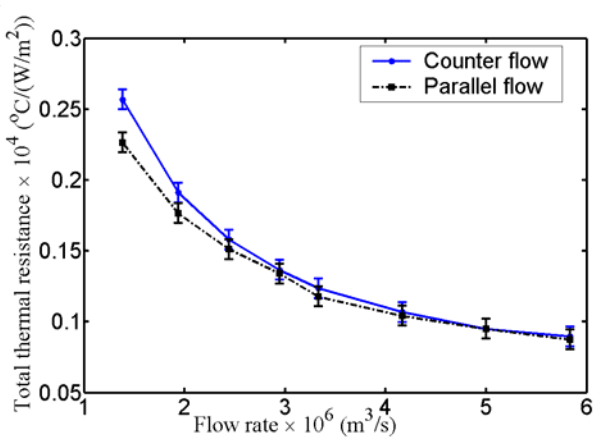

Fig. 8 Total thermal resistances for parallel flow and Counter flow with equal flow rate at each of the two microchannels layers (Wei et al., 2004)

3.2 Two Phase Implementations

Meso-scale flow loops utilizing two-phase flow may be buoyancy driven, or may involve forced circulation. In applications where the orientation of the heat source is fixed, the use of gravity driven fluid circulation of the coolant may be achieved by utilizing a two-phase thermosyphon. In applications involving changes in orientation a forced circulation scheme is necessary.

3.2.1 Thermosyphons With Boiling Enhancement Structures:

Most of the earlier implementations have utilized a single chamber construction, also termed a wickless heat pipe. Additional placement flexibility in space constrained applications may be obtained by using a remote heat exchanger, as in Fig. 4. A compact evaporator is essential for successful implementation of a thermosyphon for chip cooling. This requires predictable onset of boiling within the evaporator, with minimal superheat excursion. For low surface tension fluids such as the dielectric fluorocarbon family, boiling enhancement structures have been successfully employed to achieve pool boiling heat fluxes of ~ 100 W/cm^2, based on the projected area, with an elimination of the boiling incipience excursion.

A boiling enhancement structure utilizing a three-dimensional network of interconnected microchannels is seen in Fig. 9. Structures of this type with somewhat larger pore sizes have been evaluated for pool boiling performance by Nakayama and co-workers (1980a, 1980b, 1982, 1984). Depending upon the material, these structures can be readily fabricated using a variety of micro manufacturing techniques, including wire electro-discharge machining, wafer dicing, and wet or dry chemical etching. Examples of structures fabricated in silicon are provided in Fig. 10 (Ramaswamy et. al, 1999). The effect of confinement on the boiling performance was investigated by starting with a larger evaporator and progressively confining the space around the boiling structure (Ramaswamy et al., 1999a). It was found that as long as the structure remained flooded with the working fluid, the boiling performance was quite good. This resulted in the development of a very compact evaporator, using a stacked boiling enhancement structure. One such thermosyphon prototype was developed for the thermal management of a desktop computer central processing unit chip, with a power dissipation of 85 W (Pal et. al, 2002). With water as a working fluid, the maximum temperature rise at the evaporator base was ~35 ^{o}C, and with FC 72 it was ~75 ^{o}C. The performance of the system was influenced by orientation, resulting in dryout when the circulation could not be maintained.

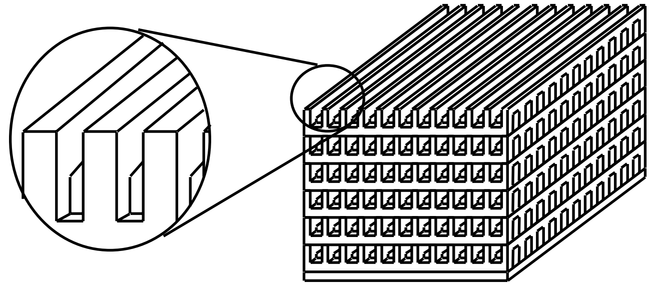

Fig.9 Stacked boiling enhancement structure

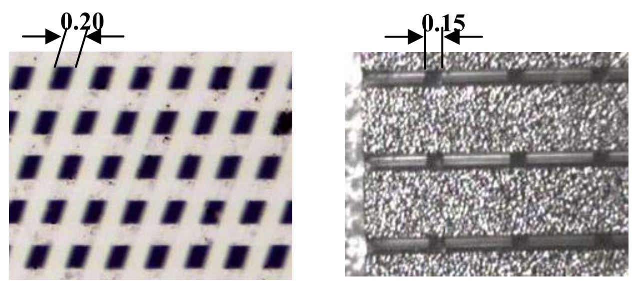

(a) **(b)**

Fig.10 Examples of boiling enhancement structures fabricated in silicon using wet etch methods (a), and wafer dicing (b), (Ramaswamy et al., 1999). The dimensions are in mm.

3.2.2 Pool Boiling Performance Model for Enhanced Structures;

Ramaswamy et al. (2003) developed a semi-analytical model to predict the bubble departure diameter, frequency, and nucleation site density for a boiling enhancement structure. The model provided improvements on existing sub-models for bubble departure diameter, evaporation within the channels, and convective heat transfer from the external surfaces of the enhanced structure.

The steps in predicting the essential parameters, leading to the total heat flux are as follows:

1) Calculate the bubble departure diameter.
2) Calculate the initial meniscus radius from the correlation developed.
3) Calculate the latent heat transfer inside the microchannel during the waiting period ($Q_{t,w}$) and also calculate the waiting period (Δt_w). After every time step, a new meniscus radius was calculated. The meniscus radius at the end of the waiting period becomes the initial value for the growth period.
4) Calculate the growth period (Δt_g).
5) Calculate the latent heat transfer inside the tunnel during the growth period ($Q_{t,g}$) by dividing the entire

growth period into small time increments and stepping through them similar to step 3.

6) Calculate the frequency of bubble departure (f) as $1/(\Delta t_w + \Delta t_g)$.
7) Calculate the total tunnel heat flux (q''_t) as $(Q_{t,w} + Q_{t,g})f / A_{ex}$, where A_{ex} is the external surface area of the structure
8) Calculate the nucleation site density.
9) Calculate the external convective heat flux (q''_{ex}) .
10) The total heat flux is calculated as $q'' = q''_t + q''_{ex}$

Comparisons with experiments revealed that the bubble departure was predicted within $\pm$ 10%, frequency within $\pm$ 30 % for all data points except a couple, nucleation site density within $\pm$ 40 % and the heat flux within $\pm$ 50 %. Results for the heat flux are provided in Fig. 11.

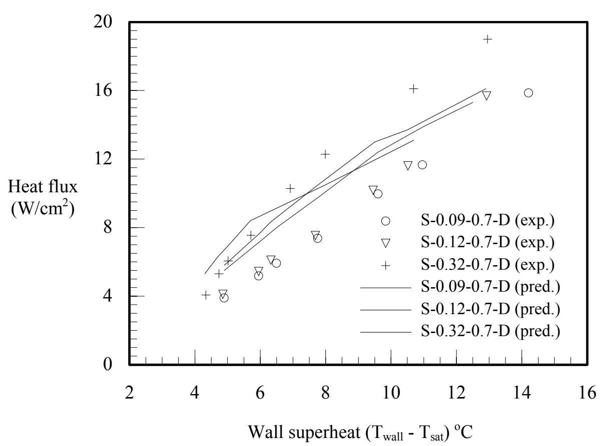

Fig. 11 Comparison of predicted and experimental heat flux for three structures (Ramaswamy et al., 2003).

***3.2.3 System Thermal Performance Model*;**

Haider et al. (2002) developed a system performance model for a two-phase thermosyphon, based on mass, momentum, and energy balances in the evaporator, rising tube, condenser, and the falling tube. A homogeneous two-phase flow model is used to evaluate the friction pressure drop of the two-phase flow driven by the available gravitational head through the loop. All two-phase flow parameters are cross-sectionally averaged, with vapor assumed to be an ideal gas in thermodynamic equilibrium with the liquid phase. The model assumes constant liquid/vapor thermophysical properties, with the exception of vapor density that varies with saturation temperature and pressure that are, inter-dependent.

The model neglects pressure drops in the evaporator and the condenser as well as the heat losses from the rising and falling tubes. The saturation temperature dictates both the heat source (chip) temperature and the condenser heat rejection capacity. Thermodynamic constraints are applied to model the saturation temperature, which also depends upon the local heat transfer coefficient and the two-phase flow patterns inside the condenser. The boiling characteristics of the enhanced structure are used to predict the chip temperature.

The model couples two distinct iterations through two key design parameters- the total two-phase mass flow rate circulating through the loop and the vapor quality at the evaporator outlet. The first iteration is based on the overall momentum balance. The sum of the friction and acceleration pressure drops in the entire thermosyphon loop must be equal to the available gravitational pressure head. This natural circulation driving force is the liquid-rich falling tube gravitational head minus the vapor-rich gravitational head of the evaporator and the rising tube. The homogeneous two-phase flow model was used to evaluate the two-phase friction pressure drops in the system.

The first iteration computes a *total* two-phase mass flow rate whose circulation through the loop would satisfy the overall pressure balance along the loop. The second iteration decomposes the *total* two-phase flow rate into the *vapor* and *liquid* parts by solving the individual mass and energy balances on the evaporator and the condenser. This also requires knowledge of the air-side natural convection characteristics of the condenser. The experimentally observed boiling characteristics of the enhanced structure are input to the model and allow wall temperature prediction for a given saturation temperature. Overall, the model determines the values of the total mass flow rate and the evaporator outlet quality that would satisfy both iterations, i.e., the overall mass, momentum and energy balance, as well as the thermodynamic constraints.

Computational predictions were made for a thermosyphon experimentally evaluated by Yuan et al. (2003). Fig. 12 shows that the variation of available gravitational head between 2272 Pa to 3452 Pa, and the total mass flow rate it is able to impose through the loop between 2.6×10^{-3} kg/s to 3.2×10^{-3} kg/s.

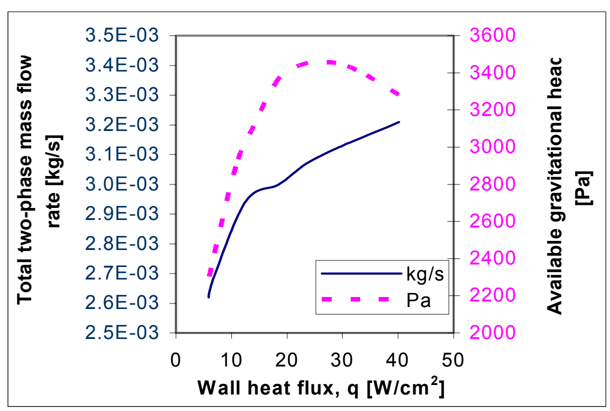

Fig. 12 Predicted available gravitational pressure head and loop mass flow rate for experimental thermosyphon (Haider et al., 2002)

3.2.4 Jet impingement and Spray Cooling Based Flow Loops:

Fabbri et al. (2005) report on the thermal performance of sprays and arrays of micro jets of de-ionized water, with an ultimate goal of developing a thermal management system where the liquid is sprayed directly on the back surface of the active die, or a heat spreader. The liquid is then collected and cooled down in a small heat exchanger, and is re-circulated in a closed loop. The impacting droplet sprays can have the form of a fixed or randomly patterned mist. If the frequency of the streams is high enough, the droplets may merge forming continuous liquid jets. After impacting the surface, the liquid droplets spread and, if the spreading area is small enough a continuous thin liquid film covering the surface is formed. If the wall superheat is high, a thin vapor layer can be present underneath the droplets or the thin liquid film. The heat transfer process is transient and involves liquid and vapor convection, thin film evaporation, and air convection. The areas not covered by the film dry out. When continuous liquid jets are employed, the liquid film covering the surface is continuous and the heat is removed mainly by convection. Evaporation from the thin film may occur at high heat fluxes or low flow rates. As pointed out by the authors, the physics governing the heat removal process by droplet sprays is very complex and not well understood. Experimental studies have been conducted in the past on sprays, but most deal with the boiling regime, which was not considered by the authors.

Experiments were conducted using HAGO nozzles and orifice plates to create droplet sprays and arrays of micro jets, respectively. The liquid jets had diameters ranging from 69 to 250 μm, arranged at pitches of 1, 2, and 3 mm. The jet Reynolds number ranged between 43 and 3813. The single phase heat transfer rates using droplets sprays and arrays of micro jets have been compared. It was found that at a flowrate of 2.87 ml/mm2 s the spray has a higher heat transfer rate than any jet configuration, while at a higher flowrate of 4.63 ml/mm^2 s jet arrays can perform as well as the spray. The micro jets arrays were found to be associated with lower energy consumption rate than the spray generated by the HAGO nozzle for the same flow rate. For equal pumping power and T_w-T_{liq} = 76°C, the jet array removed heat fluxes as high as 240 W/cm^2, while the spray could only handle 93 W/cm^2.

A closed loop cooling module employing impinging jets was tested. It consisted of three major components: an orifice plate for forming jets or a nozzle to form the spray, a container to hold the nozzle, the heat source and the cooling liquid, which also served as a heat exchanger to the ambient, and a pump which re-circulated the coolant. A remote heat exchanger was not utilized in this study, although it could be incorporated to reduce the real estate requirements near the heat source. The authors suggest that a fan could be used to improve the heat transfer to the ambient, and allow the use of a smaller container. An impinging jet cooling module was designed and tested. Heat fluxes as high as 300 W/cm^2 at 80°C surface temperature could be removed using a system which includes a 436 array of microjets of water of 140 μm diameter impinging on a diode of area 5.0387 mm^2.

Horacek et al. (2005) investigate the heat transfer mechanism for a single nozzle spray cooling of a array of micro heaters with varying amounts of dissolved gas. Total 96 micro heaters made of Platinum were formed on a 500 μm fused silica substrate. The heaters are controlled by Wheastone bridge feedback circuits to achieve uniform temperature in the range of 30 to 110^{o}C. The maximum surface heat flux capable is 250 W/cm^2. A high speed digital camera capable of acquiring 512x512 pixel images at 100 fps was used to record images by viewing through the silica substrate. Areas of liquid-solid contact were obtained using the total internal reflection (TIR) technique. Using a right angle prism attached under the silica substrate, incident light at the solid-vapor interface will be reflected almost completely which produces bright region on the image. At the solid-liquid interface the light travels through the liquid and scatters into the vapor space which results low intensity area (dark) area in the image. The images of the heater lines were filtered out during image processing.

Results were obtained with the spray nozzle oriented normal to the microheater array located 17 mm from the surface. The flow rate of the spray was set at 32 ml/min resulting 3.67 atm in pressure drop across the nozzle for the working fluid FC-72. It was found that the presence of dissolved as increased the effective subcooling of the liquid and shifted the spray cooling curves to higher wall super. The CHF was also found to increase consequently. Visualization revealed that the substrate surface was almost completely wet by liquid at low wall superheat. As wall superheat increases, the dry regions increase in frequency and size ultimately producing isolated pool of liquid. Near CHF the heater surface was covered by intermediate-sized droplets (150 μm or smaller) resulted from incident droplets. Statistical examination of the images revealed that the wetted surface area decreases monotonically with the increases in wall superheat. It is interesting to note that the contact line length (CLL) measured in the visualization suggested direct correlation with the heat flux. In fact as the wall superheat increase the CLL will increase until a maximum is obtained which correspond to the CHF. The CLL will decrease with Wall superheat subsequently. The authors further suggested manipulate the contact line length in the future to determine whether the dominant heat transfer mechanism is thin-film heat transfer or transient conduction into the liquid sublayer as in pool boiling.

Amon et al. (2005) describe the development of embedded droplet impingement for integrated cooling of electronics (EDIFICE), an integrated droplet impingement cooling device, employing latent heat of vaporization of dielectric fluids. Microfabricared microspray nozzles were fabricated to produce 50–100 μm droplets, coupled with surface texturing on the backside of the chip to promote droplet spreading and effective evaporation. A thermal management test vehicle simulating a notebook PC system was developed. The integrated droplet impingement cooling system consisted of a cooling test bed, a microdiaphragm liquid pump, a coolant reservoir, and a fin-integrated condenser. The condenser, which was mounted on the back of the display panel, was made of a 13.75 mm thick aluminum plate 316 by 254 mm, with 58 aluminum fins. The fluidic interconnections were made of plastic tubes with 3.175 mm inner diameter. To provide uniform cooling within a confined chamber, a new swiss-roll orifice, which had a diameter of 460 μm and slot width of 40 μm was developed. A silicon nozzle plate with 737 swiss-roll orifices was bonded with the inlet and swirl chip to provide atomized droplets in the prototype tests. The coolant used in all prototype tests was the dielectric fluid HFE-7200. The inlet coolant subcooling was about 50°C. The pressure of the cooling chamber was maintained at about 1 atm; hence, the saturation temperature of the coolant was kept at 76°C.

At 11.1 g/cm^2min, the silicon swiss-roll micronozzles generated fully developed droplet streams at each micronozzle. At 33.2 g/cm^2min, a uniform heat flux of 45 W/cm^2 was removed using HFE- 7200 as the coolant. By circulating water in a hermetic enclosure at a reduced system pressure heat transfer results of evaporative spray cooling on a microtextured silicon surface were also obtained. The backside of the chip was textured using deep reactive ion etching to increase spreading in order to decrease the film thickness and to provide nucleation sites to promote boiling. Three different surface textures were investigated. All microstructures were fabricated on a chip of 25.2 by 25.2 mm. The liquid film breakup heat flux for the finer-stud surface was 42.1 W/cm^2, which was comparable to the limiting heat flux in the HFE prototype testing. However, the flow rate in water tests was significantly lower, being only 4.64 g/cm^2min.

Heffington et. al (2000) describe and characterize a compact two-phase thermal management device in which thin-film evaporation on the hot surface was achieved using surface droplet atomization. Vibration-induced droplet atomization (VIDA) is a process in which small liquid droplets are produced within a sealed heat transfer cell and are propelled onto the heated surface. The VlDA technique involves the violent break-up of thin liquid layers on the vibrating surface of a piezoelectrically driven membrane that is operated at resonance. The air-side heat transfer to the ambient utilizes fins on the cell, or a liquid cooling loop coupled to an air side heat exchanger.

In recent studies by Heffington and Glezer (2004), liquid was supplied to the atomizer at a controlled rate using an integrated miniature piezoelectric pump thereby enabling orientation insensitive cell operation. The impact of the atomized droplets on the heated surface forms a thin film that evaporates continuously. The resulting vapor was condensed both on the internal surfaces of the heat transfer cell and on the surface of the atomized droplets. The condensate was collected and returned to the atomizer module by the integral diaphragm pump. The addition of a synthetic jet effectively regulates the transport of the atomized droplets to the heated surface and the transport of the vapor away from the surface. The jet was contained within the cell, and the jet fluid was a mixture of air and vapor within the cell.

3.2.5 Microchannel Flow Loops:

A number of recent studies have investigated transport in microchannels, since they form the basic flow geometry utilized in meso-scale two-phase forced convection heat sinks. An extensive review on the subject of boiling and two-phase flow in micro-channels and micro-channel structures has been provided by Ghiaasiaan and Abdel-Khalik (2001). Some of the more recent studies are summarized here.

Wu and Cheng (2003) carried out visualizations and measurement on flow boiling of water in parallel silicon microchannels of trapezoidal cross-section. Two sets of parallel microchannels, having hydraulic diameters of 158.8 and 82.8 μm, respectively, were used. For the larger channel, for an inlet water temperature of 30 ^oC, incipient boiling near the channel exit for atmospheric discharge was observed for a heat flux of 12 W/cm^2 and a fluid mass flux of 19.1 g/cm^2s. Their visualizations showed that once boiling heat was established, two-phase flow and single-phase liquid flow appeared alternatively with time in the microchannels. Large-amplitude, long period fluctuations with time in wall temperatures, fluid temperatures, fluid pressures, and fluid mass flux, were measured. The fluctuation periods were found to be dependent on channel size, heat flux, and mass flux, being 31 s and 141 s, for the larger and smaller channels respectively. Slug flow and churn flow occurred more frequently in smaller microchannels under the experimental conditions of q”=7.83 W/cm^2 and mass flux of 16.8 g/cm^2 s. Bubbly flow, which was not observed in previous microchannel papers, was observed for both microchannels.

Qu and Mudawar (2002) measured the incipient boiling heat flux in a copper heat sink containing 21 rectangular microchannels of 231 x 713 μm cross-section using de-ionized water with inlet velocities of 0.13–1.44 m/s, inlet temperatures of 30, 60, and 90^{o}C, and an outlet pressure of 1.2 bar. Using a microscope, boiling incipience was identified when bubbles were first detected near the outlet of the microchannels. They found that these bubbles grew and departed into the liquid flow instead of collapsing locally as in larger channels. Both the incipient boiling heat flux and the associated wall superheat increased with increasing inlet velocity and decreasing inlet temperature. The incipient heat flux increased approximately from 10 to 180 W/cm^2 with the wall superheat increasing approximately from 3 to 21^{o}C as the water velocity was increased from 0.15 to 1.2 m/s at an inlet water temperature of 30^{o}C. A numerical solution was obtained to predict the incipient boiling heat flux, which was found to be in reasonable agreement with their experimental data.

Qu and Mudawar (2003a-2003c) experimentally studied pressure drop and heat transfer characteristics of water flow boiling in a rectangular micro-channel heat sink containing 231 x 713 μm cross-section micro-channels. Previous macro-channel models and empirical correlations were assessed and deemed unable to accurately predict pressure drop or heat transfer in micro-channel heat sinks. An annular flow model was developed to describe the heat transport characteristics of the heat sink, which showed excellent predictive capability for their data.

Jiang et al. (2001) conducted visualization studies of water flow boiling in triangular silicon micro-channels having hydraulic diameters of 26 and 53 μm respectively. Annular flow was the dominant flow pattern at moderate to high heat fluxes. The bubbly flow regime, common to macro flow boiling systems, was never observed. Zhang et al. (2002) studied water flow boiling in rectangular silicon micro-channels with hydraulic diameters from 25 to 60 μm and aspect ratios from 1.0 to 3.5. Nucleation and small bubble growth were observed inside the micro-channels at low heat fluxes, but annular flow became dominant at high heat fluxes. The bubbly and slug flows typically observed in macrochannels were absent in their experiments.

Hetsroni et al. (2001) investigated flow boiling of water in the silicon triangular microchannels having hydraulic diameters of 103 and 129 μm respectively. Their experiments were carried out at heat fluxes in the range of 8– 36 W/cm^2 and Reynolds numbers from 20 to 75. Two types of periodic flow patterns, annular flow and dry steam flow were found. No fluctuation data on pressure or temperature were reported. Hetsroni et al.(2002) studied flow boiling of dielectric liquid Vertel XF in a microchannel heat sink containing 21 parallel triangular micro-channels having a base dimension of 250 μm. The flow in the microchannels alternated between single-phase liquid and elongated vapor bubbles. The low-amplitude/short-period fluctuations in the pressure drop and outlet fluid temperature were attributed to the growth and collapse of vapor fraction.

Steinke and Kandlikar (2004) characterized the thermal and hydraulic performance of six parallel trapezoidal microchannels with a hydraulic diameter of 207 μm. The adiabatic single-phase friction factor for laminar flow of water in microchannels was accurately described by the established relationship for larger conventional channels. A flow reversal was observed under certain conditions in microchannels. The vapor interface moved in a direction counter to the bulk fluid flow. A maximum heat flux of 930 kW/m^2 was achieved, with heat transfer coefficients as high as 192 kW/m^{2}K. A decreasing trend in two-phase heat transfer coefficient, with an increasing quality was detected. These trends are consistent with a nucleate boiling dominant flow. The trends seen in flow boiling data in microchannels are different from those observed in larger diameter tubes. The role of nucleate boiling was seen to be more predominant than previously thought.

Pokharna et al. (2004) evaluated a thermal management system consisting of a microchannel evaporator, coupled with a remote heat exchanger for microprocessor cooling. Both single phase and two-phase pumped loops were considered, with the objective of incorporating these within laptops, desktops and server computers. Degassed water was utilized as the working fluid under sub-atmospheric conditions, with saturation temperature in the range 65^{o}C – 70^{o}C. Evaporator thermal resistance of under 0.1 ^{o}Ccm^2/W were achieved for single phase and two phase operation, with the channel width of ~90 μm. A correlation for Nusselt number for the annular and stratified two-phase flow regimes was developed, with the data agreeing better with the latter. It was argued that if microchannels below hydraulic diameters of 100 μm could be economically fabricated, single phase convection would provide performance comparable to annular two-phase flow, without the added complexities of two-phase instabilities.

3.3 Two Phase Heat Spreaders

There is a growing need to develop thin, high thermal conductivity heat spreaders for electronics thermal management. These can be utilized in space constrained portable systems to achieve an effective reduction in heat flux. In high performance desktop systems, such heat spreaders can be combined with air cooled heat sinks to increase the overall heat removal rates. Emerging applications such as three-dimensional electronics also require ultra-thin, high effective thermal conductivity heat spreaders. Recent efforts have focused on the development of both advanced high thermal conductivity materials such as diamond films, as well as thin flat heat pipes. A heat spreader utilizing the boiling enhancement structure of Fig. 9 was investigated by Murthy et al. (2002, 2003, 2004). Murthy et al. (2004) also provide a review of the recent literature on heat spreaders, including microfabricated flat heat pipes.

3.3. 1 Heat Spreader Utilizing Enhanced Boiling:

The boiling based heat spreader is illustrated in Fig. 13. The heating is supplied in the central region of the thin flat spreader containing a working fluid. This results in the boiling of the fluid from the boiling enhancement structure. The bubbles move towards the periphery of the device, where they condense. A vigorous circulation of the liquid and vapor is maintained by the microfabricated boiling enhancement structure of the type illustrated in Fig. 9.

Vapor and liquid trains are formed within the microchannels, and the differential in capillary effects across each vapor or liquid slug is thought to produce the driving force. Since these trains are different from the transport of vapor and liquid in a heat pipe or vapor chamber, these devices are not limited by the typical capillary limits of a heat pipe. The microchannel dimensions in our studies so far were selected for dielectric working fluids such as fluorocarbons. One of the attractive features of this device for portable applications is that by a proper selection of dimensions of the evaporator and condenser, and the thickness, it is possible to have the performance largely independent of orientation over a large range of angles.

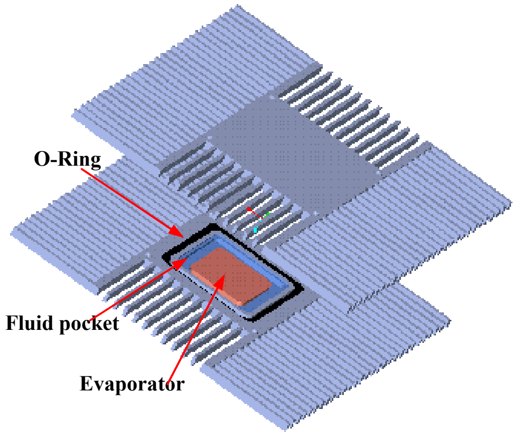

Fig. 13 *Schematic of 2-phase spreader plate with peripheral fins (Murthy et al. (2004))*

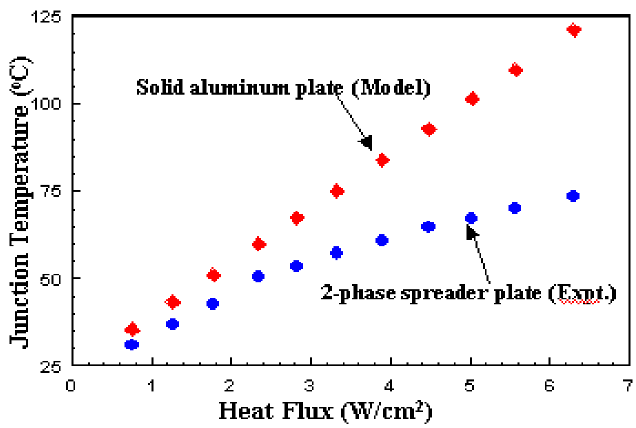

Fig. 14 *Performance evaluation of the thin plate heat spreader under natural-air cooled conditions at an ambient of 23 °C. At a heat flux of 6.3 W/cm^2, the junction temperature of the two-phase heat spreader was less than that of a solid aluminum plate by 47.1 °C (Murthy et al. (2004)).*

3.3. 2 Pulsating Heat Pipe Based Spreaders:

These devices consist of a serpentine tube or channel, whose ends may or may not be interconnected. There is at least one evaporator and one condenser zone. No internal wick is utilized, in contrast to a conventional heat pipe. The meandering tube is evacuated and partially filled with the working fluid. Internal temperature gradients result in two-phase flow instabilities and thermal transport. By embedding the serpentine tube within a thin plate a heat spreader can be formed. A recent review of the operating characteristics of these devices and their applications to electronics thermal management is provided by Groll and Khandekar (2004).

4 REMOTE HEAT EXCHANGE

A key bottleneck in the miniaturization of a pumped loop system is the air-side heat exchanger. It can account for 75% of the thermal resistance in an evaporator and 95% in a condenser for typical refrigeration applications (Jacobi and Shah, 1998). Jacobi and Shah (1998) advocate a fundamental understanding of the air flow in the complex passages of compact heat exchangers. These flows can be steady or unsteady; laminar or turbulent; internal, external or periodic; and developing and developed.

As pointed out by Harris et al. (2002), the current state of the art in compact air-side heat exchangers is driven by automotive radiators. The common measure of performance for these is the heat transfer per unit frontal area, per unit temperature difference in the inlet temperatures of the coolant (water-glycol) and air. For current state-of-the-art radiators, performance up to 0.31 W/cm^{2}K can be achieved. These radiators are relatively thick (1-2 cm). Harris et al. (2000) designed cross-flow micro heat exchangers 5.1 cm by 5.1 cm, of thickness 0.1 cm – 0.2 cm in plastic, ceramic and aluminum. It was found that the heat transfer per unit frontal area of the micro heat exchangers was 2-4 times less than innovative car radiators. However, the heat transfer per unit volume and per unit weight were 2-8 times those of existing radiators. Design calculations indicated a capability of 33.3 W/cm^3 for a micro heat exchanger of plastic and 59.4 W/cm^3 for aluminum, versus 9 W/cm^3 for current innovative car radiators. A plastic micro heat exchanger was fabricated using the LIGA microfabrication process, precision micromachining, alignment, and bonding.

Mahalingam et al. (2004) have reported on the use of synthetic microjects for creating low profile air-side heat sinks. These devices utilize a piezoelectrically activated diaphragm to create highly targeted zero mass injection, but finite momentum transport flows. Heat dissipations of ~10 W is possible in very low form factor type portable electronic products. Larger heat sinks can be designed for heat removal capability of over 100 W.

5 PUMPING TECHNOLOGY STATUS

A miniature/micro pump is a key component of the mesoscale flow loop for electronics cooling, particularly when gravity driving force is absent. The current status of the pumping technology for meso-scale flow loops is reviewed.

5.1 Micropump/miniature Pump

An extensive review of micropumps can be found in Laser and Santiago (2004). The current survey will focus on the micropumps that can potentially be applied for electronics cooling.

Since the 1980s tremendous efforts have been devoted to micropump research. Micropumps can be generally categorized as displacement type where moving boundaries exert pressure on the working fluid and dynamic type where energy can be added to the working fluid continuously (Laser and Santiago, 2004.). Examples of displacement micropumps include piezoelectric actuated reciprocating pump and thermopneumatic pumps. These pumps typically work in two strokes: intake stroke and discharge stroke. Dynamics pumps include electrohydrodynamic pumps, electroosmotic pumps and magnethydrodynamic pumps.

Most of the earlier micropumps are of the reciprocating displacement type where external forces are applied on a diaphragm to discharge or intake the fluid. Fig. 15 illustrates a typical reciprocating displacement micropump. The driver, diaphragm, chamber and valves are the main components of such a pump; therefore, the performance of the pump is determined by the characteristics of these components as well as the fluid properties. Based on the driving mechanism, the driver can be piezoelectric, thermopneumatic, or electrostatic. Controlled by external inputs, the driver vibrates at a certain frequency which causes the diaphragm to deform accordingly. The maximum changes in chamber volume in one cycle and the frequency determine the flow rate and pressure head generated. Clearly, for a given driving force, the displacement of the diaphragm is a function of the thickness, diameter and material Young's modulus. Fig 16 (a) and (b) depict the variations of the centerline displacement of the diaphragm with the applied force and diaphragm diameter for 100 µm and 10 µm thick silicon respectively, assuming the actuation force is uniformly applied on the diaphragm and the diaphragm is completely clamped at the perimeter. The displacement increases rapidly with diameter for both thicknesses. Also shown in Fig 16 is the resonant frequency of the diaphragm, which decreases sharply with increasing diameter. These two trends imply an optimum diameter for a given thickness and actuation force to maximize the flow rate output.

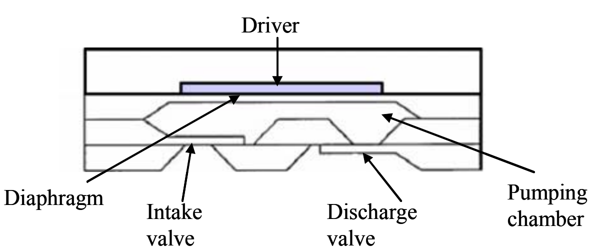

Fig 15 Schematic of a typical reciprocating micropump (Laser and Santiago, 2004)

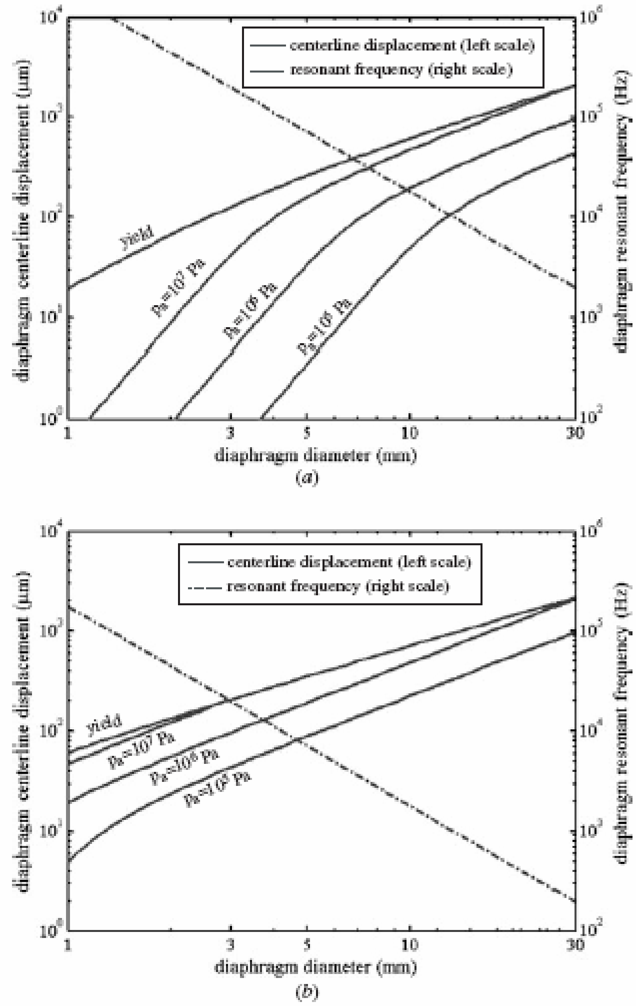

Fig 16 Effects of diaphragm diameter on the characteristics of pump (Laser and Santiago, 2004)

Piezoelectric micropumps are probably the most common micropumps reported so far. Smits (1990) reported a peristaltic piezoelectric micropump constructed in glass-Si-glass with three pump chambers. The working principle is schematically shown in Fig. 17. Piezoelectric actuators drive the chamber in 120 degree phase difference producing a net flow from inlet to outlet. This pump does not need any valve to regulate the flow direction. Operating at 100 V and 15 Hz this pump produces a maximum flow rate 100 fµl/min and a maximum pressure of 600 Pa.

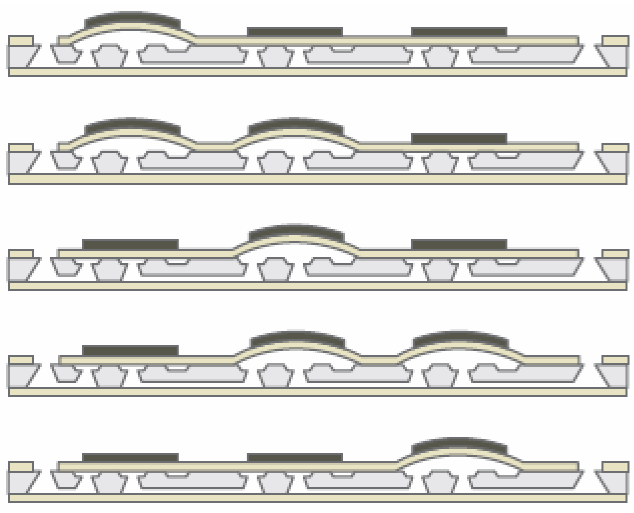

Fig. 17 Working principle of a peristaltic micropump, (Smits, 1990)

Stehr et al. (1996) reported a reciprocating micropump using a bimorphic piezoelectric cantilever To drive the diaphragm. The maximum flow rate and pressure head is 1.5 ml/min and 17 kPa respectively when operating at 190 Hz and 200 V. Li et al. (2000) reported a piezoelectric stack actuation micropump. For silicone oil the micropump could generate a maximum flow rate 3 ml/min and maximum pressure head 300 kPa operating at 1.2 kV and 3.5 kHz. Another common actuation mechanism is electrostatic actuation. Zengerle et al (1995) discussed a reciprocating micropump driven by electrostatic force. The maximum flow rate for water was 0.85 ml/min and the maximum pressure was 29 kPa when operating at 200 V and 800 Hz

Schomburg et al. (1994) reported a thermopneumaticlly driven micropump capable of delivering air at a maximum flow rate of 44 μl/min and the maximum achievable pressure head is 3.8 kPa at 15 V and 5 Hz. Thermo-pneumatcally driven micropumps often use low-modulus diaphragm materials. In the micropump reported in Schomburg et al., a 2.5 μm polyimide layer is used as the diaphragm. Tsai and Lin (2002) reported a thermal capillary pump driven by bubbles generated through electrical heating. Operating at 20 V and 400 Hz this pump delivered isopropyl alcohol at a maximum 45 μl/min and the maximum pressure possible was 400 Pa.

The second type of micropumps are dynamic pumps where an external field is applied to the fluid which cause the fluid to flow. In a electrohydrodynamic (EHD) pump, electric field is applied to a dielectric fluid field where ions are introduced by induction, conduction or injection. Richter et al. (1991) reported an injection EHD micropump constructed of Si-Si. It could deliver ethanol at a maximum flow rate of 14 ml/min and a maximum possible pressure of 0.43 kPa at 600 V.

An electroosmotic (EO) pump is schematically shown in Fig 18. In EO flow, mobile ions in the diffuse counter-ion layer of the electric double layer are driven by an externally applied electrical field. These moving ions drag along bulk liquid through viscous force interaction. Bulk flow is thus introduced in the direction of the applied field.

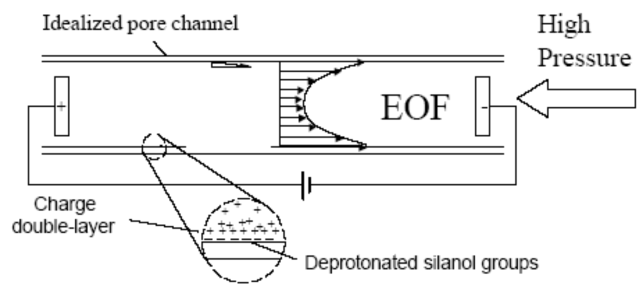

Fig. 18 Schematic of an electroosmotic pump (Yao et al., 2001)

An EO pump reported in Yao et al. (2001) used sintered glass frit as the insert in the pump chamber. Using Borate buffer as the working fluid, the maximum flow rate reported was 7 ml/min and the maximum possible pressure head was 250 kPa. Laser et al (2003) presented an EO micromachined pump capable of delivering Borate buffer at a maximum flow rate of 0.17 ml/min and maximum pressure of 10 kPa at 400 V. Si-glass was used as the chamber insert. One of the issues with EO pump is the electrolyte by-product gases. A Pt catalyst is introduced to recombine the gases back into water. Fig 19 shows an EO pump with the gas recombination system. This pump is capable of delivering a maximum of 33 ml/min and a maximum pressure of 1.3 bar at 100 V. Compared with other micropumps, the size of this pump is relatively large and should be considered as a mini-pump instead.

For meso-scale flow loops for electronic cooling, micropumps with high flow rate and pressure head are highly desirable. Fig 20 compares the performance of five pumps in terms of the maximum flow rate and maximum pressure. The low cost and simple thermopneumatic pump can only provide low flow rate and low pressure head. Electrostatically driven micropumps are very promising as they are very compact and can be fully micromachined and can work at high frequency. Further research is required to improve in performance. EO pumps and piezoelectric pumps are similar in performance. Perhaps the most prominent EO pump is the one reported in Yao et al (2003) which can deliver a maximum flow rate of 33 ml/min. EO pump also features high maximum pressure. Piezoelectric stack driven pumps can also generate high pressure but the flow rate is limited (3 ml/min, Li 2000). It appears that current micro-pumps are still not sufficient for electronics cooling. Further research in this area is necessary.

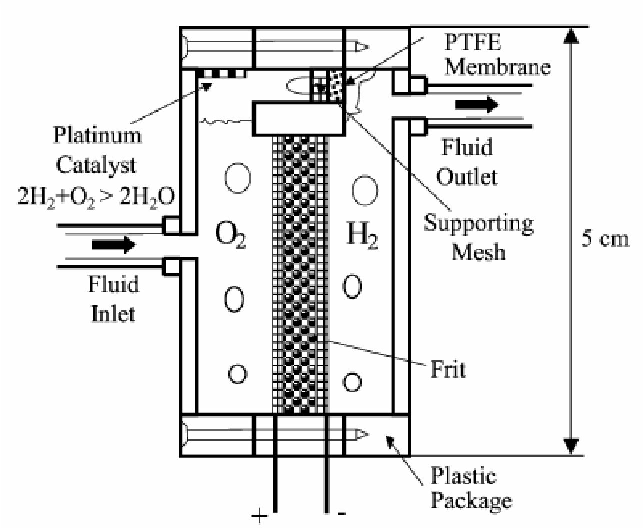

Fig. 19 Schematic of an electroosmotic pump (Yao et al. , 2003)

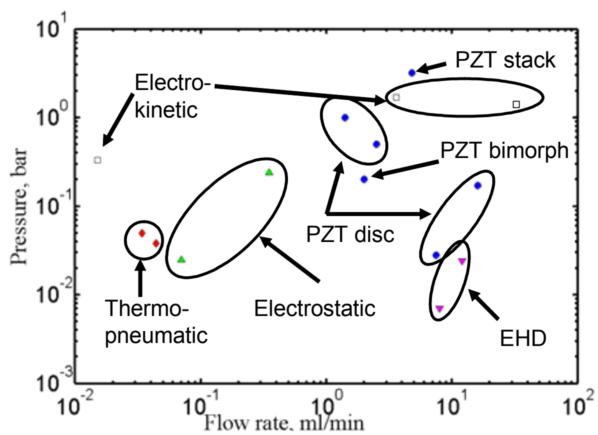

Fig 20 Characteristics of different micropumps

6 FUTURE CHALLENGES

While micro and meso-scale single phase liquid or two-phase thermal management systems have been demonstrated to provide superior thermal performance that can adequately meet cooling goals of future electronic systems, these are currently not widely utilized. A number of challenges need to be met in order for this situation to change in the near future. The manufacturing of the individual components (the chip to working fluid, and working fluid to ambient heat exchangers and compact pumps) and their integration need to be done in a cost effective and reliable manner. The chip to working fluid heat exchanger may be fabricated in silicon for direct attachment, or metal such as copper for attachment to a heat spreader. Low cost manufacturing of high aspect ratio microchannels and fluid inlet and exit plenums in these materials, and their bonding to the chip or heat spreader are critical. These manufacturing and assembly steps must be carried out at low enough temperatures, so as not to adversely impact the chip electrical functionality. For in-direct attachment of thermally mismatching cooling devices, high performance and reliable thermal interface materials have to be used, the thermal resistance of which compromise the overall cooling performances considerably.

Low cost, compact, and high reliability liquid pumping solutions are needed for all single phase forced convection loops, and also for loops employing forced convection boiling. Also required are modular, leak proof fluidic interconnects that can be customized for specific applications. The on-chip or on-package fluid connection components and the interfaces between have to be able to survive the assembly steps. For overall optimization of the size of the flow loop, the air side heat exchanger is a critical element. Relatively small amount of attention has been paid to this. There is an immediate need for micro and meso-scale heat exchangers that can provide significant gains in the volumetric heat removal rates compared to today's state-of-the-art automotive heat exchangers.

Acknowledgements: The authors acknowledge support for some of the research reported here under the DARPA HERETIC Program and Intel Corporation. Our current efforts are supported by the National Science Foundation Microsystems Packaging Research Center, and the Interconnect Focus Center Research Program at Georgia Tech, supported by the Microelectronics Advanced Research Corporation (MARCO), its participating companies, and DARPA under contract 2003-IT-674.

REFERENCES

Amon, C.H., Yao, S.C., Wu, C.F., Hsieh, C.C., 2005, "Miccroelectromechanical System-Based Evaporative Thermal Management of High Heat Flux Electronics", J. Heat Transfer, Vol. 127, pp. 66-75.

Baviere, R., Ayela, F., Person, S. Le. and Favre-Marinet, M., 2004, "An Experimental Study of Water Flow in Smooth and Rough Rectangular Micro-channels", 2nd International conference on microchannels and minichannels, Rochester, New York, 221-228

Horacek B., Kiger K.T., and Kim J., 2005, "Single nozzle spray cooling heat transfer mechanisms", International Journal of Heat and Mass Transfer, Vol 48, pp.1425-1438

Chen K.C., Ayón,A.A., Zhang X., and Spearing s. M, 2002, "Effect of Process Parameters on the Surface Morphology and Mechanical Performance of Silicon Structures After Deep Reactive Ion Etching (DRIE)", J. Microelectromechanical Systems, 11, pp. 264-275

Fabbri, M., Jiang, S., Dhir, V.K., 2005,"A Comparative Study of Cooling of High Power Density Electronics Using Sprays and Microjets", J. Heat Transfer, Vol. 127, pp. 38-48.

Foll H, Christophersen M., Carstensen J., and Hasse G., 2002, "formation and application of porous silicon," Material Science and Engineering, Vol. R 39, pp.93-141.

Ghiaasiaan, S. M., and Abdel-Khalik, S. I., 2001, ''Two-Phase Flow in Microchannels,''
Advances in Heat Transfer, Academic Press, New York, 34, pp. 145–254.

Groll, M. and Khandekar, S., 2004,"State of the Art on Pulsating Heat Pipes", Second International Conference on Microchannels and Minichannels, Rochetser, New York, pp. 33-44.

Haider, S.I., Joshi, Y.K., and Nakayama, W., "A Natural Circulation Model of the Closed Loop, Two-phase Thermosyphon for Electronics Cooling," J. Heat Transfer, Vol. 124, (2002), 881-890.

Harris, C.; Kelly, K.; Tao Wang; McCandless, A.; Motakef, S., 2002, **"**Fabrication, modeling, and testing of micro-cross-flow heat exchangers", Journal of Microelectromechanical Systems, Vol. 11, pp. 726 - 735

Heffington, S.N., W.Z. Black, and A. Glezer, 2000, "Vibration-Induced Droplet Cooling of Microelectronic Components," ITHERM 2000 Proceedings**,** Vol. 2, Las Vegas, NV, pp.328- 332.

Heffington, S.N., and Glezer, A., 2004 , "Two-Phase Thermal Management Using a Small-Scale, Heat Transfer Cell Based on Vibration-Induced Droplet Atomization", Inter Society Conference on Thermal Phenomena (ITherm), Las Vegas, Nevada.

Hetsroni, G., Mosyak, A., Segal, Z., 2001, "Nonuniform temperature distribution in electronic devices cooled by flow in parallel microchannels", IEEE Trans. Components Packaging Technol. 24 (1), pp. 17–23.

Hetsroni, G., Mosyak, A., Segal, Z., Ziskind, G., 2002, "A uniform temperature heat sink for cooling of electronic devices", Int. J. Heat Mass Transfer 45, pp. 3275–3286.

Jacobi, A.M., and Shah, R.K., 1998,"Air-Side Flow and Heat Transfer in Compact Heat Exchangers: A Discussion of Enhancement Mechanisms, Heat Transfer Engineering, Vol. 19, pp. 29-41.

Jiang, L., Wong, M., Zohar, Y., 2001, "Forced convection boiling in a microchannel heat sink, J. Microelectromech. Syst. 10 (1), pp. 80–87.

Laser D J *et al,* 2003, "Silicon electroosmotic micropumps for IC thermal management,' Proc. Transducers '03 (Boston, MA)

Laser D. J. and Santiago J. G., 2004, "A review of micropumps," Journal of Micromechanics and Microengineering, 14, pp. R35-R64

Lee, P. and Garimella, S. V., 2003, "Experimental Investigation of Heat Transfer in Microchannels", HT2003-47293, Proceedings of HT2003, ASME summer heat transfer conference.

Lehmann V., 1993, "The physics of macropore formation in low doped n-type silicon", Journal of Electrochemical Society, Vol 140, pp. 2836-2843

Li H Q *et al,* 2000, "A high frequency high flow rate piezoelectrically driven MEMS micropump," *Proc. 2000* Solid-State Sensor and Actuator Workshop (Hilton Head, SC)

Liu, D. and Garimella, S. V., 2002, "Investigation of Liquid Flow in Microchannels", 8th AIAA/ASME Joint Thermophysics and Heat Transfer Conference, St. Loius, Missouri, Paper No. AIAA 2002-2776

Mahalingam, R., Rumigny, N., Glezer, A., 2004, *IEEE Transactions on Components Parts and Manufacturing Technology*, Vol. **27**.

Mehendale, S. S., Jacobi, A. M., and Shah, R. K., 2000, ''Fluid Flow and Heat Transfer at Micro and Meso-Scales With Application to Heat Exchanger Design,'' Appl. Mech. Rev., Vol. 53, No. 7, pp. 175–193.

Murthy, S.S., Joshi, Y., and Nakayama, W., 2002, "Single Chamber Compact Thermosyphons With Micro-fabricated Components", IEEE Transactions on Components and Packaging Technologies, Vol. 25, 156-163.

Murthy, S., Joshi, Y., and Nakayama, W., 2003, "Orientation Independent Two-Phase Heat Spreaders for Space Constrained Applications", Microelectronics Journal, Vol. 34, pp. 1187-1193.

Murthy, S., Joshi, Y. and Nakayama, W., 2004, "Two-Phase Heat Spreaders Utilizing Microfabricated Boiling Enhancement Structures", Heat Transfer Engineering Vol. 25, pp. 26-36.

Nakayama, W., Daikoku, T., Kuwahara, H., and Nakajima, T., 1980a, "Dynamic Model of Enhanced Boiling Heat Transfer on Porous Surfaces, Part I: Experimental Investigation," J. Heat Transfer, Vol. 102, 445-450.

Nakayama, W., Daikoku, T., Kuwahara, H., and Nakajima, T., 1980b, "Dynamic Model of Enhanced Boiling Heat Transfer on Porous Surfaces, Part II: Analytical Modeling," J. Heat Transfer, Vol. 102, 451-456.

Nakayama, W., Daikoku, T., and Nakajima, T., 1982, "Effetcs of Pore Diameters and System Pressure on Saturated Pool Boiling Heat Transfer From Porous Surfaces", J. Heat Transfer, Vol. 104, 286-291.

Nakayama, W., Nakajima T., and Hirasawa, S., 1984, "Heat Sink Studs Having Enhanced Boiling Surfaces For Cooling Microelectronic Components", ASME Paper No.84-WA/HT-89.

Pal, A., Joshi, Y., Beitelmal, M. H., Patel, C. D. and Wenger, T., 2002, "Design and Performance Evaluation of a Compact Thermosyphon", IEEE Transactions of Components and Packaging Technologies, Vol. 25 (4), 601-607.

Papausky , Brazzle J., Swerdlow H., and Frazier A.B., 1998, "A low temperature IC-compatible process for fabricating surface micromachined metallic microchannels," J. Microelectromechanical Systems, Vol. 7, pp. 267-273

Pokharna, H., Masahiro, K., DiStefano, E., Mongia, R., Barry, J., Crowley, C., Chen, W., and Izenson, M., 2004, "Microchannel Cooling in Computing Platforms: Performance Needs and Challenges in Implementation", Second International Conference on Microchannels and Minichannels, Rochester, New York, pp. 109-118.

Qu, W., and Mudawar, I., 2002, "Prediction and Measurements of Incipient Boiling Heat Flux in Microchannel Heat Sinks", Int. J. Heat Mass Transfer, Vol. 45, 3933–3945.

Qu, W., and Mudawar, I., 2003a, ''Measurement and prediction of pressure drop in two-phase micro-channel heat sinks,'' Int. J. Heat Mass Transfer, **46**, pp. 2737–2753.

Qu, W., and Mudawar, I., 2003b, ''Flow Boiling Heat Transfer in Two-Phase Micro-Channel Heat Sinks-I. Experimental Investigation and Assessment of Correlation Methods,'' Int. J. Heat Mass Transfer, **46**, pp. 2755–2771.

Qu, W., and Mudawar, I., 2003c, ''Flow Boiling Heat Transfer in Two-Phase
Micro-Channel Heat Sinks-II. Annular Two-Phase Flow Model,'' Int. J. Heat Mass Transfer, **46**, 2773–2784.

Qu, W., Yoon, S.M., Mudawar**,** I, 2004, "Two-Phase Flow and Heat Transfer in Rectangular Micro-Channels", J. Electronics Packaging, Vol. 126, pp. 288-300.

Ramaswamy, C., Joshi, Y., Nakayama, W., and Johnson, W.B., 1999a, "Compact Thermosyphons Employing Microfabricated Components", Microscale Thermophysical Engineering, Vol. 3, 273-282.

Ramaswamy, C., Joshi, Y., Nakayama, W., and Johnson, W.B., 1999b, "Thermal Performance of a Compact Two-Phase Thermosyphon: Response to Evaporator Confinement and Transient Loads," J. Enhanced Heat Transfer, Vol. 6, 279-288.

Ramaswamy, C., Joshi, Y., Nakayama, W., Johnson, W.B., 2003, "Semi-Analytical Model for Boiling from Enhanced Structures", Int. J. Heat Mass Transfer, Vol. 46, 4257-4269.

Richter A, Plettner A, Hofmann K A and Sandmaier H 1991 "A micromachined electrohydrodynamic (EHD) pump, Sensors Actuators A **29** 159–68

Saito, N., 1984, "Recent electrical discharge machining techniques in Japan", Bulletin of Japanese Society of Precision Engineering, Vol 18, pp. 117-125.

Schomburg W K *et al* 1994, "Microfluidic components in LIGA technique," J. Micromech. Microeng. **4** 186–91

Sharp, K.V., Adrian, R.J. and Beebe, D.J., 2000, "Anomalous Transition to Turbulence in Microtubes", MEMS 2, 461-466

Smits J G, 1990, "Piezoelectric micropump with 3 valves working peristaltically," Sensors Actuators A **21** 203–6

Stehr M, Messner S, Sandmaier H and Zengerle R, 1996, "The VAMP: a new device for handling liquids or gases," Sensors and Actuators A **57** 153–7

Steinke, M.E., Kandlikar, S.G., 2004, "An Experimental Investigation of Flow Boiling Characteristics of Water in Parallel Microchannels", J. Heat Transfer, Vol. 126, pp. 518-526.

Tsai J H and Lin L 2002, "A thermal-bubble-actuated micronozzle-diffuser pump," J. Microelectromech. Syst. **11,** 665–71

Tuckerman, D.B. and Pease, R.F.W., 1981, "High performance heat-sinking for VLSI", IEEE electron Device Letter 2, pp. 126-129

Viswanath R., Vijay W., Watwe A., and LebonheurV., "Thermal performance challenges from silicon to systems," Intel Technology J., Q3, 2000.

Wei X.J., Joshi Y.K. and Patterson, M.K., 2005, "Experimental and Numerical Study of Stacked Microchannel Heat Sinks for Liquid Cooling of Microelectronic Devices, to be submitted.

Wei X.J., Joshi Y.K. and Patterson, M., 2004, "Stacked microchannel heat sinks for liquid cooling of microelectronics", Proceedings of IMECE, paper number IMECE2004-62509

Wu, H.Y., Cheng, P., 2003, "Visualization and Measurements of Periodic Boiling in Silicon Microchannels", Int. J. Heat Mass Transfer, Vol. 46, pp. 2603–2614.

Xu, B., Ooi, K. T., and Wong, N. T., 2000, “Experimental Investigation of Flow Friction for Liquid Flow in Microchannels”, International Communications in Heat and Mass Transfer, 27, 1165-1176.

Yao S, Huber D E, Mikkelsen J C and Santiago J G, 2001,” A large flow rate electroosmotic pump with micron pores,” Proc. 2001 ASME Int. Mechanical Engineering Congress and Exposition (New York, NY)

Yao S H, Hertzog D E, Zeng S L, Mikkelsen J C and Santiago J G, 2003, “Porous glass electroosmotic pumps: design and experiments,” J. Colloid Interface Sci. 268, 143–53

Yuan, L., Joshi, Y.K., and Nakayama, W., 2003, “Effect of Condenser Location and Imposed Circulation on the Performance of a Compact Two-Phase Thermosyphon”, Microscale Thermophysical Engineering, Vol. 7, 163-179.

Zeighami, R., Laser, D., Zhou, P., Asheghi, M., Devasenathipathy, S., Kenny, T., Santiago, J., and Goodson, K., 2000, “Experimental Investigation of Flow Transition in Microchannel Using Micro-resolution Particle Image Velocimetry”, Proceedings of ITHERM 2000, Volume II, 148-153

Zengerle R, Ulrich J, Kluge S, Richter M and Richter A 1995, “A bidirectional silicon micropump Sensors Actuators A 50, 81–6

Zhang, L., Koo, J.M., Jiang, L., Asheghi, M., Goodson, K.E., Santiago, J.G., 2002, “Measurements and modeling of two-phase flow in microchannels with nearly constant heat flux boundary conditions”, J. Microelectromech. Syst. 11 (1), pp. 12–17.

Zhu X.S., Choi J.W., Cole R, and Ahn,C.H., 2002, “A new laser micromachining technique using a mixed mode ablation approach”, IEEE MEMS 2002, pp.152 – 155.